Chromophore-Protein Interactions in the Anthozoan Green Fluorescent Protein asFP499

Karin Nienhaus,* Fabiana Renzi,† Beatrice Vallone,† Jörg Wiedenmann,‡ and G. Ulrich Nienhaus*§
*Department of Biophysics, University of Ulm, 89069 Ulm, Germany; †Department of Biochemical Sciences, University of Rome "La Sapienza", 00185 Rome, Italy; ‡Department of General Zoology and Endocrinology, University of Ulm, 89069 Ulm, Germany; and §Department of Physics, University of Illinois at Urbana-Champaign, Urbana, Illinois 61801

ABSTRACT Despite their similar fold topologies, anthozoan fluorescent proteins (FPs) can exhibit widely different optical properties, arising either from chemical modification of the chromophore itself or from specific interactions of the chromophore with the surrounding protein moiety. Here we present a structural and spectroscopic investigation of the green FP asFP499 from the sea anemone *Anemonia sulcata* var. *rufescens* to explore the effects of the protein environment on the chromophore. The optical absorption and fluorescence spectra reveal two discrete species populated in significant proportions over a wide pH range. Moreover, multiple protonation reactions are evident from the observed pH-dependent spectral changes. The x-ray structure of asFP499, determined by molecular replacement at a resolution of 1.85 Å, shows the typical β-barrel fold of the green FP from *Aequorea victoria* (avGFP). In its center, the chromophore, formed from the tripeptide Gln^{63}-Tyr^{64}-Gly^{65}, is tightly held by multiple hydrogen bonds in a polar cage that is structurally quite dissimilar to that of avGFP. The x-ray structure provides interesting clues as to how the spectroscopic properties are fine tuned by the chromophore environment.

INTRODUCTION

Anthozoa display a wide array of colors to which fluorescent proteins (FPs) contribute in a major way (1–5). From this protein family, the green FP from *Aequorea victoria* (avGFP) is arguably the most popular representative, and its structural (6,7) and spectroscopic (8,9) properties have been extensively characterized. The polypeptide chain of avGFP is folded into an 11-stranded β-barrel encasing a distorted α-helix that runs along the axis of the barrel. The helix is interrupted by the tripeptide Ser^{65}-Tyr^{66}-Gly^{67} from which the flat, conjugated π-electron system of the intrinsic chromophore forms by an autocatalytic, posttranslational modification that involves a nucleophilic attack of the Gly^{67}-Nα on the Ser^{65} carbonyl to produce an imidazolin-5-one intermediate; subsequent dehydrogenation of the Cα-Cβ bond of Tyr^{66} by molecular oxygen yields the 4-(*p*-hydroxybenzylidene)-5-imidazolinone chromophore (10,11). The thermodynamically very stable β-barrel fold provides a rigid environment that endows the chromophore with a high fluorescence quantum yield and shields it from diffusional quenchers (7).

Recent years have witnessed the development of FP-based biosensors for a great variety of applications in life sciences research, including gene expression, subcellular protein distribution and trafficking, protein-protein interactions and H^+, and halide and metal ion concentration determinations (9,12–16). The spectral properties of the chromophore are controlled by the surrounding protein moiety, which can be modified specifically by genetic engineering. A variety of avGFP mutants have been created, emitting blue, cyan, and yellow light (9,17–19), for use in multi-color labeling or Förster resonance energy transfer experiments. The FP toolbox was further extended by the discovery of FPs in non-bioluminescent anthozoa. Among these, species with entirely novel properties were identified, including red fluorescence emission, as in DsRed (20–22) and eqFP611 (23,24), and light-induced green-to-red conversion, as in Kaede (25,26) and EosFP (27–29).

Further modification and optimization of the optical properties of anthozoan FPs, especially their photostability, brightness, and excitation and emission wavelengths (21,30–33), are highly desirable for many applications. For a rational engineering of these marker proteins, however, a detailed understanding of the structure-function relationship is a prerequisite. To this end, we have embarked on a program to identify and characterize, on the molecular level, a large variety of FPs from anthozoan sources. In this work, we present the x-ray structure at 1.85-Å resolution of asFP499, a green FP from the sea anemone *Anemonia sulcata* var. *rufescens* (3) that has only 18.7% sequence identity with avGFP. With its emission maximum at 499 nm, it takes an intermediate position between cyan FPs (~485 nm) and truly green FPs (~510 nm) naturally found in anthozoa (4,34). The structural data have been complemented with a detailed study of its optical absorption and fluorescence properties. Analysis of the interaction of the chromophore with the surrounding protein moiety enables us to elucidate the structural basis for its distinct spectral properties.

Submitted April 18, 2006, and accepted for publication August 30, 2006.

Karin Nienhaus and Fabiana Renzi contributed equally to this work.

Address reprint requests to G. Ulrich Nienhaus, Dept. of Biophysics, University of Ulm, 89069 Ulm, Germany. Tel.: 49-731-502-3050; Fax: 49-731-502-3059; E-mail: uli@uiuc.edu.

0006-3495/06/12/4210/11 $2.00

doi: 10.1529/biophysj.106.087411

MATERIALS AND METHODS

Protein expression, purification, and crystallization

Cloning of the gene coding for asFP499 into *Escherichia coli* was described previously (3). Mutant $Asp^{158}Asn$ was created using the Quikchange mutagenesis kit (Stratagene Europe, Amsterdam, The Netherlands). Custom designed primers were ordered from MWG-Biotech (Ebersberg, Germany). The proteins were expressed in *E. coli* strain BL21/DE3 and purified using a TALON metal affinity resin (BD Biosciences, Clontech, Palo Alto, CA). Crystals of asFP499 were grown at 20°C in 30% polyethylene glycol (PEG) 4000, 0.1 M Tris pH 8.5, 0.2 M $MgCl_2$, using the hanging drop vapor diffusion technique. The crystals were transferred to cryosolvent (26% glycerol, 30% PEG 4000, 0.1 M Tris, pH 8.5, 0.2 M $MgCl_2$) and flash frozen in liquid nitrogen.

Data collection and structure determination

X-ray diffraction data were taken at the ELETTRA synchrotron source (Trieste, Italy) using an x-ray wavelength $\lambda = 1.0$ Å and a temperature of 100 K. Reflections up to a resolution of 1.85 Å were collected on a marCCD detector (MAR Research, Hamburg, Germany). The crystals belonged to space group P21, with unit cell parameters $a = 81.658$ Å, $b = 113.437$ Å, $c = 104.420$ Å, $\beta = 94.26°$. Diffraction images were indexed, reduced, and scaled with the HKL package (35). The structure was solved by molecular replacement with the program AmoRe (36), using the structure of eqFP611 from *Entacmaea quadricolor* (23,24), which has 55.8% sequence identity with asFP499, as the search model. The model contained two tetramers in the asymmetric unit. Model building was carried out manually by using QUANTA (37) and COOT (38); 5% of the reflections were flagged for FreeR cross validation data refinement. Several cycles of manual rebuilding and subsequent refinement were performed. The chromophore was built into both the 2Fo-Fc (contoured to 1.0 and 1.5 σ) and the Fo-Fc (contoured to 3.0 σ) electron density maps. Ramachandran analysis was performed with PROCHECK (36). The geometry of the final model is excellent, with 91.2% of the residues in the most favored regions of the Ramachandran plot, 8.1% positioned in other allowed regions, and only 0.7% in generously allowed regions (Table 1). Water molecules were modeled into large experimental electron density features in hydrogen-bonding distance of appropriate partners by using COOT (38). Buried areas were calculated with AreaIMol (36). Graphics were produced with PyMol (39). The data collection and refinement statistics are summarized in Table 1. Data deposition: The atomic coordinates and structure factors have been deposited in the Protein Data Bank (PDB), www.pdb.org (PDB ID code 2C9I).

Optical spectroscopy

Absorption and fluorescence spectra at 20°C were collected on asFP499 samples dissolved in 100 mM sodium citrate/sodium phosphate, sodium phosphate, and sodium carbonate buffers for the pH ranges <5, 5–8.5, and >8.5, respectively. For data collection at cryogenic temperature (12 K), samples were prepared in 75%:25% (v/v) glycerol/phosphate buffer at pH 8 and kept in a closed-cycle helium cryostat (model 22, CTI Cryogenics, Mansfield, MA) equipped with a Lake Shore Cryotronics (Westerville, OH) model 330 digital temperature controller. Absorption spectra at 20°C were collected on a Cary 1 spectrophotometer (Varian, Darmstadt, Germany) at a resolution of 1 nm; absorption spectra at 12 K were taken on an OLIS-modified Cary 14 spectrometer (On-Line Instrument Systems, Bogart, GA) at a resolution of 0.4 nm. Fluorescence excitation and emission spectra were measured with a SPEX Fluorolog II spectrofluorometer (Spex Industries, Edison, NJ) with the excitation line width set to 0.85 nm; the emission was recorded with 2.2-nm resolution. Emission spectra were corrected for the detector response.

TABLE 1 Crystal parameters of asFP499 and data collection and refinement statistics

Crystal parameters and data collection statistics	
Temperature (K)	100
Space group	P1 21 1
Cell dimensions (Å,°)	$a = 71.880$; $b = 135.126$; $c = 95.071$; $\beta = 106.93$
Unit cell volume (Å^3)	883,372.81
Solvent content (%)	43.9
Resolution (Å)	1.85
Total no. of observations	1,532,588
No. of unique observations	128,068
Mosaicity	0.94
Multiplicity	5.5
Data completeness (%)	87.3 (81.4)
I/σ	17.5
R_{merge}*	0.05 (0.19)
Data refinement statistics	
Nonhydrogen atoms	
Protein	14,048
Chromophore	192
Water	1596
Resolution (Å)	1.85
R_{factor}†	0.21
R_{free}	0.27
rmsds from ideality	
Bond lengths (Å)	0.01
Bond angles (°)	1.91
Ramachandran plot	
Most favored (%)	91.2
Allowed region (%)	8.1
Generously allowed region (%)	0.7
Disallowed (%)	0.0
B-factors (Å^2)	
Overall	24
Average main chain	21
Average side chain	25
Average chromophore	19

The values in parentheses are for the highest resolution bin (approximate interval 0.15 Å).
*$R_{merge} = \Sigma((I_{hkl} - \langle I_{hkl}\rangle)^2)/\Sigma(I^2_{hkl})$.
†$R_{factor} = \Sigma_{hkl} \| |F_o| - F_c| / \Sigma_{hkl} |F_o|$ for all data except for 5%, which was used for free R calculation.

RESULTS

Quaternary structure

The asymmetric unit of asFP499 contains two identical tetramers related by a noncrystallographic symmetry. They are arranged as dimers of dimers, so that two types of subunit interfaces can be distinguished; they are denoted as antiparallel (between subunits A/B and C/D) and perpendicular (between subunits A/C and B/D) interfaces according to the mutual orientations of the main axes of the β-barrels. Both interfaces involve hydrophobic and hydrophilic interactions. The antiparallel interface is stabilized in its center by hydrophobic interactions between the facing pair Leu^{122}-Leu^{122} and between Val^{93} and Val^{101} of different chains. The interface is further reinforced by three hydrogen bonds: one

provided by the Ser[103]-Ser[103] pair, and the other two formed between Tyr[21] of one chain and Thr[177] of the other chain at the edge of the interface. The perpendicular interface is stabilized by a π stacking interaction between the Phe[173] benzyl side chains of both subunits. Additional hydrophobic contacts are provided by Phe[191] of one chain and Pro[42] of the other chain, although the Pro[42] carbonyl likely weakens this interaction. Two salt bridges exist between Arg[150] and Glu[97] of different subunits. The interfacial contacts are compiled in Table 2 together with the total surface areas of the interfaces.

Tertiary structure

The monomeric subunits within the tetramers are essentially identical, as judged from the average root mean-square deviation (rmsd) of the Cα atoms of 0.21 Å. The overall backbone topology shows the typical 11-stranded β-barrel fold, with the central α-helix interrupted by the chromophore. The N-terminal end (residues 1–7) forms a lid on the same barrel, thereby assisting in shielding the interior of the can from the environment, whereas the C-terminal tail (residues 220–228) wraps around the other barrel in the A/B dimer. The asFP499 structure is similar to that of avGFP, with an rmsd of the Cα atoms of 1.15 Å. Backbone structural differences between asFP499 and avGFP are most pronounced in the region corresponding to amino acids 138–141 (143–146 in avGFP) and in the loop region formed by amino acids 195–206 (204–216 in avGFP).

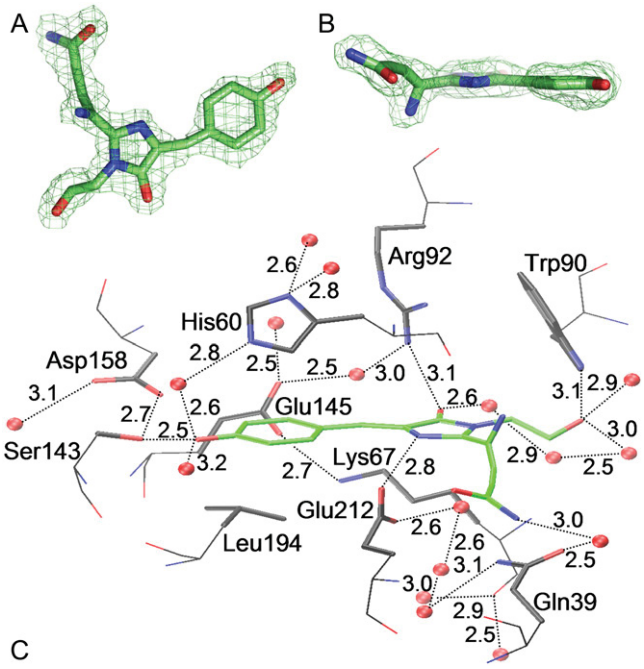

FIGURE 1 (*A*) Top and (*B*) side view of the electron density map of the asFP499 chromophore and its environment, contoured at 1.2 σ. (*C*) Close-up of the asFP499 chromophore (*green*, carbon; *red*, oxygen; *blue*, nitrogen) and surrounding residues (*black*, carbon; *red*, oxygen; *blue*, nitrogen). The backbone structures are plotted as lines; the side chains are accentuated. Water molecules are plotted as red spheres. Hydrogen bonds are represented by dashed lines. Distances are given in angstroms.

The chromophore and its environment

The chromophore of asFP499 is a planar resonance system formed autocatalytically by residues Gln[63], Tyr[64], and Gly[65] (Fig. 1, *A* and *B*). It consists of an imidazolinone ring generated by cyclization between the Gln[63]-C′ and the Gly[65]-Nα atoms and the Tyr[64] hydroxyphenyl group, which is made coplanar with the imidazolinone due to dehydrogenation insaturation of its Cα-Cβ bond. Whereas there is a glutamine in the first position of the tripeptide instead of the serine in avGFP, the asFP499 chromophore is essentially identical to that of avGFP, including the *cis* configuration at the Tyr[64]-Cβ, which is encountered more frequently than the *trans* conformation.

The chromophore of asFP499 is tightly encased within the β-barrel by a hydrogen-bond network involving polar and charged residues and altogether 10 structural waters within a

TABLE 2 Interfacial contacts and total buried areas for avGFP and asFP499

	avGFP				asFP499			
A/B (antiparallel)	Hydrophobic		Hydrophilic		Hydrophobic		Hydrophilic	
	A Ala[206] Leu[221]	B Phe[223] Phe[223]	A Ser[208] Asn[149] Ser[202]	B Tyr[39] Glu[142] Asn[144]	A Leu[122] Val[93]	B Leu[122] Val[101]	A Ser[103] Tyr[21]	B Ser[103] Thr[177]
Total buried area*	5737 Å^2 (33.2% of total dimer area*)				6213 Å^2 (33.0% of total dimer area)			
A/C (perpendicular)					Hydrophobic		Hydrophilic	
					A Phe[173] Phe[191]	C Phe[173] Pro[42]	A Arg[150]	C Glu[97]
Total buried area					5665 Å^2 (33.1% of total dimer area)			

*The total dimer surface area is the sum of the surface areas of the monomers. The buried area is the interaction surface between the monomers, calculated with the program AreaIMol as implemented in the CCP4 suite (36).

distance of 5 Å from the imidazolinone oxygen. Fig. 1 *C* displays the chromophore cage, with potential hydrogen-bond interactions represented by dashed lines. Their lengths in angstrom units are also given in the figure. The side chain of Gln^{63} is hydrogen bonded to amino acid Gln^{210} (3 Å, not shown in Fig. 1 *C*) and via a water molecule also to Gln^{39}, which in turn is connected to the Glu^{212} carboxyl by a chain of three water molecules. The backbone carbonyl of Gly^{65} interacts with the Nε of Trp^{90}. The highly conserved residues Arg^{92} and Glu^{212} have been implicated as being crucially involved in the mechanism of autocatalytic chromophore formation (6,40,41). The Arg^{92} guanidinium group hydrogen bonds to the Tyr^{64}-derived carbonyl oxygen, whereas Glu^{212} is positioned within hydrogen-bonding distance to the heterocyclic ring nitrogen, as has been observed earlier for yellow avGFP variants (42). In close proximity to the imidazolinone ring, the presumably positively charged Lys^{67} forms a salt bridge with the negatively charged Glu^{145}. The Tyr^{64} hydroxyl is engaged in hydrogen-bonding interactions with the Ser^{143} hydroxyl and two structural water molecules. The Ser^{143} hydroxyl also forms a short hydrogen bond to Asp^{158}. The hydroxyphenyl ring of Tyr^{64} is packed against Leu^{194} from below. Frequently, a histidine imidazole is found at this location, for example in eqFP611 (23,24,43) and EosFP (27,28,44), and its π-stacking interaction with the Tyr^{64} hydroxyphenyl moiety has been suggested to cause a red shift of the chromophore resonance (9,45). In asFP499, a histidine, His^{60}, is found on the opposite side of the hydroxyphenyl group, where its imidazole side chain is held in place in an almost perpendicular orientation with respect to the phenyl ring by hydrogen bonds of its ring nitrogens to three water molecules (Fig. 1 *C*).

Overview of spectroscopic properties

The optical absorption, excitation, and emission spectra of asFP499 at pH 5, 8, 10.5, and 12 taken at ambient temperature are presented in Fig. 2. The excitation spectra were recorded by monitoring the emission at 530 nm; the emission spectra were collected with excitation at 480 nm. To display the different spectra within the same plot and to compare their relative intensities, the absorption spectra were normalized to unity at 280 nm. The excitation spectra were scaled to the absorption spectra to match the peak intensity of the band near 480 nm. The emission spectra were scaled to maintain the relative fluorescence intensities at different pH.

In addition to the ultraviolet (UV) band at 280 nm from aromatic amino acid side chains, the absorption spectra contain two bands in the visible region at ~400 and ~480 nm. In avGFP, the corresponding transitions are denoted as A and B bands; they have been assigned to the neutral (phenol) and anionic (phenolate) forms of the chromophore, respectively (9,46,47). As for wild-type avGFP, significant proportions of both species exist over a wide pH range. Remarkably, the spectral area of the protonated species even increases toward high pH. The absorption bands are rather broad, with full widths at half-maximum of ~75 and 45 nm for the A and B bands, respectively.

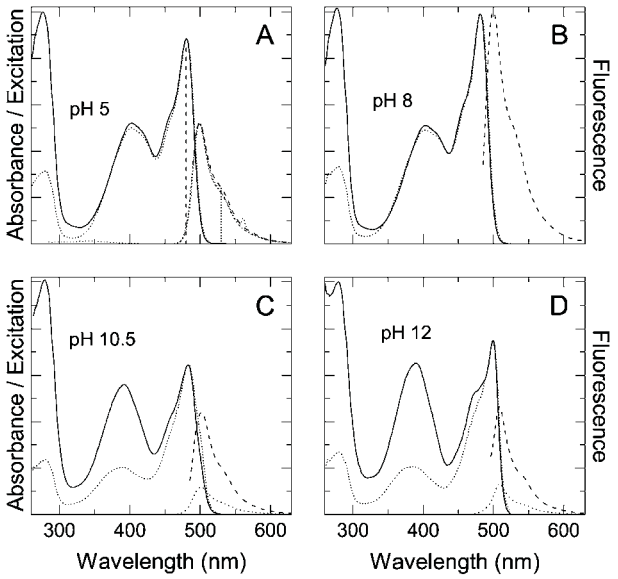

FIGURE 2 Absorption (*solid*), excitation (*dotted*), and emission (*dashed*) spectra of asFP499 at (*A*) pH 5, (*B*) pH 8, (*C*) pH 10.5, and (*D*) pH 12. In panel *A*, emission spectra collected upon excitation at 280 and 400 nm are included (*short dashed/dash-dotted lines*). In panels *C* and *D*, emission spectra collected upon excitation at 380 nm are included (*short-dashed lines*). The absorption spectra have been scaled to unity at 280 nm. The excitation spectra have been adjusted to match the maximal absorbance at ~480 nm. All emission spectra have been scaled by the same factor. The dashed (*dotted*) vertical lines in panel *A* indicate the excitation wavelength of the emission spectra (the monitoring wavelength of the excitation spectra).

The excitation spectra essentially track the absorption spectra in the A and B bands below pH 8, indicating that the fluorescence emission at ~500 nm can equally well be excited in both peaks. At high pH (pH 10.5 and 12), fluorescence excitation becomes less efficient in the A band (Fig. 2, *C* and *D*). The small excitation peak at 280 nm indicates weak Förster transfer from aromatic residues to the chromophore. The fluorescence emission is maximal in the pH range 6–8 and drops toward lower and higher pH values. For pH $<$ 10, the peak of the emission band is close to 499 nm for excitation at 480 nm; no other fluorescence emission bands are observed upon excitation at 280, 380, and 400 nm, with the exception of the very weak tryptophan fluorescence at ~340 nm included in Fig. 2 *A*. At pH $>$ 10, a red-shifted form emerges, with absorbance and emission peaks displaced by 18 and 10 nm to the red, respectively (Fig. 2 *D*).

In contrast to the wild-type protein, the chromophore of mutant $Asp^{158}Asn$ exists solely in the anionic form. Its absorption and excitation spectra are identical within the experimental error. At pH 8, the absorption peaks at 483 nm; the emission maximum is at 501 nm. All peak wavelengths are summarized in Table 3.

TABLE 3 Absorption and emission maxima of avGFP, asFP499, and asFP499 mutant Asp^{158}Asn

FP	pH	$\lambda_{max.\ abs.}$ (A) (nm)	$\lambda_{max.\ abs.}$ (B) (nm)	$\lambda_{max.\ em.}$ (nm)
avGFP*		398		460/508
			475	504
asFP499	Acid denatured	381		
	4	402	478	499
	6–8	403	480	499
	10	390	480	499
	12	389	498	509
	Base denatured		446	
Asp^{158}Asn	Acid denatured	381		
	4		480	501
	6–9		483	501
	Base denatured		449	

*Data taken from Wood et al. (41).

Vibrational substructure

To better resolve the vibronic structure of the absorption and emission bands, a sample at pH 8 was cooled to 12 K (Fig. 3 *A*), and the second derivatives were calculated to determine peak positions to within ±0.5 nm (Fig. 3 *B*). The Stokes shift, which is the displacement between the absorption and emission bands, decreases from 19 nm (~800 cm^{-1}) at room temperature (Fig. 2 *B*) to 7.2 nm (~300 cm^{-1}) at 12 K. For the B form, the spectral sidebands in absorption and emission are mirror images, reflecting their vibronic nature. We locate the position of the 0-0 transition at the midpoint between the main absorption and emission maxima (48). The displacement of the sidebands from the 0-0 transition yields an average frequency of low frequency phonons of 160 ± 30 cm^{-1} and high frequency vibrations of 860 ± 30 and 1520 ± 30 cm^{-1}. The vibronic substructure in the absorption spectrum of the A form is similar to the one observed for avGFP (48). However, the lacking emission spectrum prevents us from locating the energy of the 0-0 transition precisely.

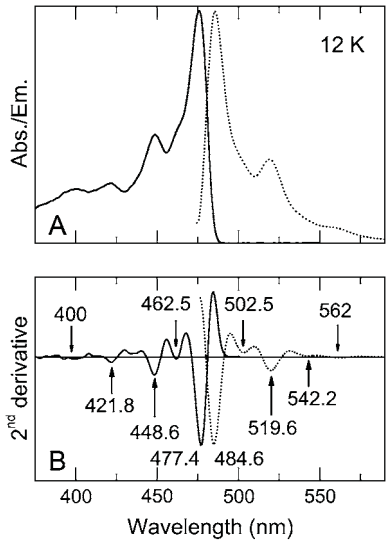

FIGURE 3 (*A*) Absorption and emission spectra of asFP499 (pH 8) at 12 K. (*B*) Second derivatives of the spectra in panel *A*. Peak positions are given in nanometers (±0.5 nm).

pH-dependent spectral changes

The absorption spectra of asFP499 display a rather complex pH dependence. Below pH 4, the protein is unstable and denatures, as indicated from the continuous development of the spectrum toward that of acid-denatured avGFP (49), with a single band peaking at 381 nm, as shown in Fig. 4 *A*. At pH 3.2, a mean lifetime (1/*e* decay) of 31 ± 1 min was obtained for the denaturation transition at 20°C (data not shown). Between pH 4 and 6, a small yet noticeable red shift and an increase of the B band absorption occurs, whereas the A band weakens but retains its shape and position (Fig. 4 *A*). As shown in Fig. 4 *B*, the peak shift of the B band with pH from 477.5 to 480.5 nm can be fitted with a simple Henderson-Hasselbalch relation, yielding a pK_a of 4.4 ± 0.1 for the protonating group. Between pH 6 and 8, the spectra are completely independent of proton concentration. Above

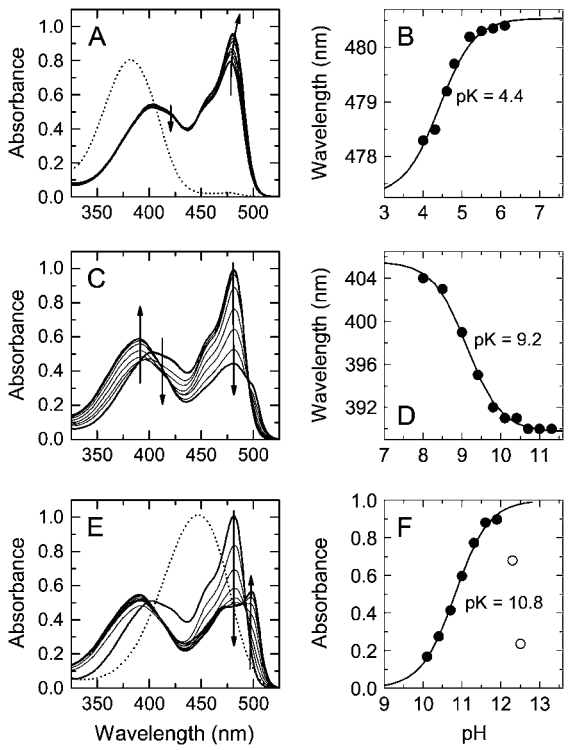

FIGURE 4 pH dependence of the absorption spectra of asFP499. Arrows indicate the change with increasing pH. (*A*) Absorption spectra in the pH range 4–6. The spectrum of the acid denatured form is included (*dotted line*). (*B*) B band peak position as a function of pH. (*C*) Absorption spectra in the pH range 8–11. (*D*) A band peak position as a function of pH. (*E*) Absorption spectra at pH values between 9 and 12. (*F*) Normalized absorbance change at 498 nm. The open symbols at pH > 12 indicate the denaturation of the protein.

pH 8, a pronounced blue shift from 404 to 391 nm is observed for the A band (Fig. 4 *C*), and moreover, the A band gains significantly in area at the expense of the B band. The pH dependence of the transition can again be modeled by a protonation of a group with $pK_a = 9.2 \pm 0.1$ (Fig. 4 *D*). By adding low-pH buffer to asFP499 samples at pH 10.5, the low-pH spectrum is readily restored (data not shown), which suggests that the protein is still fully intact in this pH region. Above pH 10, a new, red-shifted band appears at 498 nm (Fig. 4 *E*). From the pH dependence of the peak amplitude of the red-shifted band, the pK_a for this protonation reaction can be determined as 10.8 ± 0.2 (Fig. 4 *F*). This species is fully developed but only transiently stable at pH 12, as the spectrum develops over time to that of the base-denatured protein characterized by a chromophore absorption at 446 nm (49). At pH 12, the mean lifetime of the red-shifted species was determined as 227 ± 10 min at 20°C (data not shown).

In Fig. 5 *A*, the absorption spectra of asFP499 mutant $Asp^{158}Asn$ are plotted between pH 3 and 6. Below pH 3.7, the acid denatured species develops (*dotted line*). The absorption band due to the anionic chromophore shifts with increasing pH from 479.5 to 483.5 nm according to a Henderson-Hasselbalch relation with $pK_a = 4.0 \pm 0.1$ (Fig. 5 *B*). In the pH range 6–9, the spectra are identical (data not shown). At higher pH, the base denatured species (*dashed line* in Fig. 5 *A*) is observed.

DISCUSSION

Despite its low sequence identity with avGFP, asFP499 features the same overall structure and similar spectroscopic properties. Whereas avGFP is monomeric except at high concentration (9,50), asFP499 forms tetramers not only in the crystal but also in solution (3), as inferred from the apparent molecular mass of 66 kDa upon elution from a Superdex 75 column under physiological conditions (27). The x-ray structure shows the typical 4-(*p*-hydroxybenzylidene)-5-imidazolinone chromophore formed from the tripeptide Gln^{63}-Tyr^{64}-Gly^{65} inside the 11-stranded β-barrel, where it is held tightly in place by many hydrogen-bonding interactions with polar and charged amino acids and structural water molecules. The optical spectrum shares a characteristic property with wild-type avGFP, namely the presence of both A and B conformers over a wide pH range. In the following, we shall discuss the optical properties and their pH-dependent changes on the basis of the structural data.

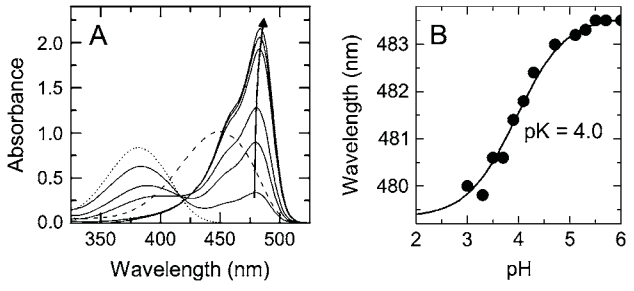

FIGURE 5 pH dependence of the absorption spectra of asFP499 mutant $Asp^{158}Asn$. (*A*) Spectra in the pH range 3–6; the spectra of the acid (*dotted line*) and base (*dashed line*) denatured forms are included. The arrow indicates increasing pH. (*B*) B band peak position as a function of pH.

Chromophore protonation states

In analogy to wild-type avGFP, the asFP499 protein shows two bands in the UV/visible spectrum over a wide pH range (Fig. 4). Although initially debated (51,52), there is now general agreement that the A and B bands are associated with the neutral and anionic states of chromophore (9). In wild-type avGFP, the A band dominates the spectrum and the B band is a minority species, with a ratio of integrated areas of ~3:1 (50). Note that this ratio does not reflect the populations because the extinction coefficients of the A and B bands can be different. A literature survey of extinction coefficients of avGFP yields estimates that range from 20,000 to 30,000 $M^{-1}cm^{-1}$ for the neutral species to 6,000–50,000 $M^{-1}cm^{-1}$ for the anionic form (9,45,53–55). However, these are the values corresponding to a molar avGFP sample containing both A and B forms; they are not the molar extinction coefficients of the two distinct species. For mutants that are almost completely shifted to the A or B form, extinction coefficients around 25,000 and 50,000 $M^{-1}cm^{-1}$ have been obtained (45). These data would yield an A/B population ratio of 6:1 for avGFP.

The structural basis of the coexistence of two conformations with different optical absorption bands was elucidated by Palm et al. and Brejc et al. (18,56). Their explanation involved a local hydrogen-bonding network adjacent to the chromophore that allows the shuttling of a proton between Glu^{222} (Glu^{212} in asFP499) and Tyr^{66} (Tyr^{64} in asFP499) via a water molecule and the side-chain oxygen of Ser^{205}. The negative charge of the deprotonated Glu^{222} stabilizes the proton on the phenol; and vice versa, the negative charge on the phenolate stabilizes the proton on Glu^{222}. It is straightforward to show that the population ratio between the two singly deprotonated forms is maintained over a pH range in which the doubly protonated or doubly deprotonated species are not significantly populated (57).

In asFP499, the two bands are similar in area in the entire pH range in which the protein is stable (Fig. 4); and remarkably, the protonated form of the chromophore becomes more dominant with increasing pH. In the structure of asFP499, amino acid Glu^{212} (corresponding to Glu^{222} in avGFP) is shown to be hydrogen bonded to the chromophore heterocycle and not connected to the phenolic oxygen at all. Therefore, proton transfer between the chromophore and Glu^{212} cannot take place. However, the structure in Fig. 1 *C* suggests an alternative explanation for the appearance of the two conformations. In addition to hydrogen bonds to two water molecules, the Tyr^{64} phenol oxygen is connected to the

Ser^{143} hydroxyl via a short hydrogen bond (2.5 Å), which in turn is hydrogen bonded to Asp^{158} (2.7 Å). The schemes in Fig. 6, *A* and *B*, show the tightly coupled system of two protonatable groups between which protons can be shuttled. The small ratio between neutral and anionic population implies that only slight differences in free energies exist between the two conformations in the electronic ground state. Upon photon absorption, this balance is disturbed. Phenols typically become more acidic upon electronic excitation (9,52); and therefore, we expect efficient excited state proton transfer (ESPT) to Asp^{158}, as is inferred from the observation that excitation in the A and B bands is equally efficient for fluorescence in the 499-nm emission band for pH < 8.

To further support the model presented in Fig. 6 by experimental evidence, we have produced the mutant Asp^{158}Asn, which has its protonatable carboxyl residue replaced by a nonprotonatable carboxamide. Evidently, protonation of Asp^{158} is a key ingredient in the proton shuttling mechanism described above. With Asn in this position, we would expect the Ser^{143} hydroxyl group only to engage in a hydrogen bond with the Tyr^{64} tyrosinate, so that the chromophore exists exclusively in the anionic form. This is indeed the case, as shown in Fig. 5 *A*.

Vibrational substructure

The detailed photophysics of the chromophore embedded in FPs presents a formidable problem to physicists and physical chemists. In addition to the electronic and vibrational excitations of the chromophore itself, interactions with the protein environment markedly affect its spectroscopic properties. Room temperature spectra are broad and rather unstructured due to structural dynamics of the chromophore and the environment. To determine the energy level schemes, it is necessary to acquire spectra at low temperature, at which the lines become much sharper. On cooling an asFP499 sample to 12 K, the lines in both the absorption and emission spectra narrow and shift significantly to the blue (Fig. 3). For the B form, the substructure of both the absorption and emission band indicates a coupling of the chromophore to vibrational modes with frequencies of 160, 860, and 1520 cm^{-1}. For avGFP, Völker and co-workers have reported similar frequencies of 220, 770, and 1508 cm^{-1} from their spectral hole-burning investigation (48). Whereas the first frequency is an effective mode representing a low frequency bath, the latter two frequencies correspond to local modes of the chromophore coupled to the electronic transition. Indeed, in the resonance Raman spectrum of avGFP, the strongest signal is at $\sim$1560 cm^{-1}, and a cluster of bands is visible around 1000 cm^{-1} (58). Isotope labeling studies have assigned the 1560-cm^{-1} band to a normal mode delocalized over the imidazolinone ring and the exocyclic double bond; the imidazolinone C-C stretching and $\rangle$C=O bending modes are located at $\sim$1000 cm^{-1} (59).

Chromophore-protein interactions

The chromophore cage contains a number of charged and polar amino acids and structural water molecules (Fig. 1 *C*). This polar environment and especially the large number of water molecules are most likely responsible for the relatively broad absorption bands (60). In addition to the negative charge either on Asp^{158} or Tyr^{64}, there is a positive charge on Arg^{92} near the imidazolinone carbonyl oxygen that draws electron density out of the imidazolinone ring. Electronic excitation is accompanied by a charge transfer from the phenol to the imidazolinone ring (52,61,62); therefore, Arg^{92} should preferentially stabilize the excited state and thus contribute to a red shift of the absorption band (9). However, Sinicropi et al. (52,61,62) have recently argued that such a

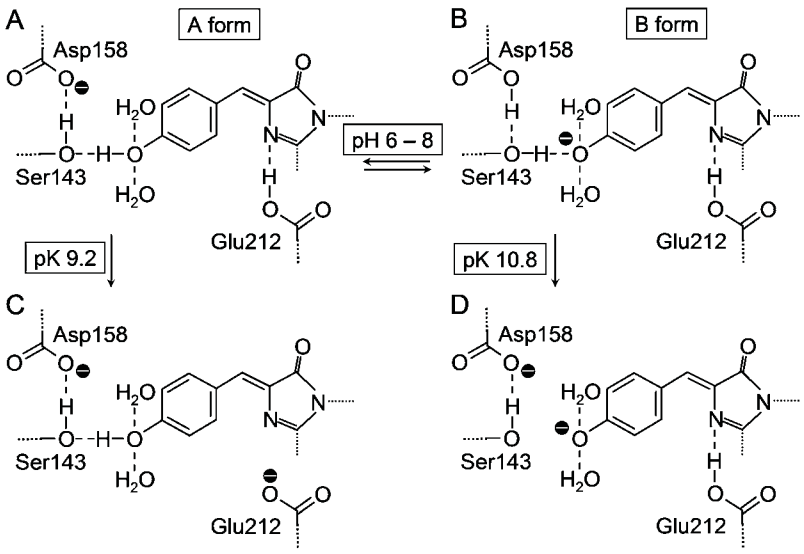

FIGURE 6 Schematic representation of the different protonation states of the asFP499 chromophore and its environment that are proposed to cause the spectral changes in Fig. 4.

red shift will only occur for an isolated chromophore-Arg system but that the protein environment ''quenches'' the effect. The x-ray structure reveals that the Tyr^{64} phenolate is hydrogen bonded to Ser^{143} and two water molecules (Fig. 1 *C*). These interactions draw electron density away from the phenolate and thereby cause a blue shift of the emission wavelength. We believe that the efficient charge stabilization on the phenolate is indeed the key structural reason for the slight blue shift of asFP499, as compared to a true green FP that emits above 500 nm. Another interesting detail of our crystal structure at pH 8 is a carboxyl oxygen atom of Glu^{212} within 2.8-Å distance of the imidazolinone nitrogen, suggesting that the neutral Glu^{212} is hydrogen bonded to the chromophore. Hydrogen bonding by the corresponding Glu^{222} has also been observed for the yellow FP mutant of avGFP (42), whereas in wild-type avGFP, the Glu^{222} side chain is anionic in the A form (46,56) and presumably the final proton acceptor in ESPT upon photoexcitation in the A band. As we have argued above, Asp^{158} likely plays the corresponding role as a proton acceptor in asFP499. Finally, Glu^{145} and Lys^{67} adjacent to the chromophore are presumably both charged and connected by a salt bridge.

Our measurements of the pH dependence of the absorbance spectra reveal a number of spectral changes that reflect alterations in the charge distribution around the chromophore. At pH $<$ 4, the protein is thermodynamically unstable, as indicated by the appearance of the peak of the acid-denatured FP at 381 nm. Above pH 4, both A and B forms are visible in similar proportion, implying that the doubly protonated (neutral) form of the Tyr^{64}/Asp^{158} system cannot be populated to a significant extent as long as the protein is in its native form. A positive charge may reside in the vicinity of the Tyr^{64}/Asp^{158} system to stabilize its negative charge, e.g., a hydronium ion or the imidazolium side chain of His^{60} on top of the Tyr^{64} phenolic ring. Indeed, the observed small red shift of the B band with increasing pH ($pK_a = 4.4$) would be consistent with the removal of a positive charge from the hydroxyphenyl side of the chromophore (Fig. 4, *A* and *B*). A positive charge in the proximity of the hydroxyphenyl ring is expected to destabilize the excited state relative to the ground state because the electron density is known to shift toward the heterocycle in the excited state (62–64). In mutant Asp^{158}Asn, a corresponding B band peak shift is visible (Fig. 5), with $pK_a = 4.0$. Similar pK_a values have been observed for the protonation of a histidine side chain in the interior of other proteins (65,66).

A further, more pronounced spectral change occurs between pH 8 and 10 (Fig. 4, *C* and *D*). With increasing pH, the peak of the A form shifts substantially (by 14 nm) to the blue, concomitant with a population transfer from the B to the A form. There are a few observations suggesting that Glu^{212} deprotonation may be responsible for these spectral changes. The proton on the Glu^{212} carboxyl is stabilized by the hydrogen bond to the imidazolinone; thus we expect a significantly increased pK_a in comparison to its value in aqueous solution ($pK_a = 4.3$) or in avGFP mutants (pK_a = 6–7) (40,46). Theoretical calculations indicate that the electron density on the lone pair of the heterocyclic nitrogen increases in the excited state (62–64). Therefore, a hydrogen bond to the heterocyclic nitrogen causes preferential stabilization of the excited state with respect to the ground state and should thus lead to a red-shifted transition. Deprotonation of Glu^{212}, by contrast, positions a negative charge close to the heterocyclic nitrogen, which has the opposite effect of destabilizing the excited state. Thereby, it should give rise to the observed blue shift of the protonated species. Interestingly, the spectral shift can only occur in the A form, which suggests that Glu^{212} deprotonation occurs only when the chromophore is protonated. The intensity of the B spectrum decreases significantly without changing shape, implying that the Glu^{212}-deprotonated A form is stabilized with respect to the B form at pH 10. Note that a decrease of the B form with increasing pH would be unreasonable when considering only the protonation equilibrium of the chromophore. Why then does Glu^{212} only deprotonate when the chromophore is in the A form? The answer is evident from the schemes of the A and B forms in Fig. 6, *A* and *B*. In the B form (Fig. 6 *B*), the Glu^{212} side chain is much closer to the negative charge on the phenolate than to the negative charge on the Asp^{158} carboxylate in the A form (Fig. 6 *C*). Therefore, the pK_a of Glu^{212} should be significantly higher in the B form, as charge interactions between the phenolate and the Glu^{212} are substantial. As shown by Scharnagl et al. (57), chromophore deprotonation causes the pK_a of the corresponding Glu^{222} in avGFP to change by $>$6 units, corresponding to $>$35 kJ/mol in free energy.

The proposed Glu^{212} deprotonation is also in agreement with the observed deviation between the excitation spectrum and the absorbance spectrum that develops between pH 8 and 10 (Fig. 2). Excitation of the 499-nm emission by absorption in the A band and hence ESPT becomes less efficient. A negative charge on the deprotonated Glu^{212} side chain will oppose the charge displacement toward the imidazolinone heterocycle upon excitation; and therefore, the tendency of the Tyr^{64} phenol to release its proton should decrease.

Above pH 10, another pronounced spectral change is apparent, characterized by a pK_a of 10.8. A red-shifted species appears at the expense of the B band, and the population of the A form increases slightly without change of the band shape. Therefore, deprotonation happens only in the B form of the chromophore. This new species slowly evolves into the base denatured form (mean lifetime ~3 h at pH 12). At pH $>$ 12, the protein is completely denatured. Red-shifted species, referred to as I states, have been observed in avGFP and mutants (48,67–70). For example, in wild-type avGFP, an I* state transiently appears when the phenolate anion is created by ESPT after excitation in the A band but is not yet solvated properly. The I* state subsequently relaxes into the B form, which involves a rotation of the Thr^{203} hydroxyl for

hydrogen bonding to the phenolate. In avGFP double mutant $Thr^{203}Val$-$Glu^{222}Gln$, the I form is even the stable state at ambient temperature, with absorption and emission maxima at 499 and 513 nm (55). In asFP499, the Ser^{143} hydroxyl can switch to Asp^{158} to form a hydrogen bond if the Asp^{158} becomes deprotonated in the phenolate form (Fig. 6 *D*). The lack of stabilization of the charge on the phenolate should give rise to the observed red shift of both absorption and emission maxima to 498 and 509 nm (Table 3). This anionic species, although in our model formally derived from the B form (Fig. 6, *B* and *D*), can even be considered as a true I form because it has maintained the hydrogen-bonding network of the A form (compare Fig. 6 *A*).

CONCLUSIONS

We have presented a spectroscopic and structural study of the green FP asFP499 from the sea anemone *Anemonia sulcata* var. *rufescens*. The x-ray structure suggests that proton shuttling between Asp^{158} and the chromophore Tyr^{64}, tightly coupled via Ser^{143}, is responsible for the presence of both neutral A and anionic B forms of the chromophore over wide pH regions, as is also observed for wild-type avGFP. This mechanism is also supported by the spectral properties of the $Asp^{158}Asn$ mutant of asFP499, in which the chromophore is exclusively in the B form. Detailed examination of the pH dependence of the optical spectra revealed charge interactions between the chromophore and the surrounding protein moiety. Different protonation states of the protein have been identified and are discussed on the basis of the molecular structure.

The work was supported by the Deutsche Forschungsgemeinschaft (SFB 569 to G.U.N.), the Fonds der Chemischen Industrie (to G.U.N.), and the Landesstiftung Baden-Württemberg (Elite-Postdoc-Förderung to J.W.).

REFERENCES

1. Wiedenmann, J. Deutsches Patent- und Markenamt, assignee. 1997. Die Anwendung eines fluoreszierenden Proteins und weiterer farbiger Proteine und der zugehörigen Gene aus der Artengruppe Anemonia sp. (sulcata) Pennant, (Cnidaria, Anthozoa, Actinaria) in Gentechnologie und Molekularbiologie. Offenlegungsschrift DE 197 18 640 A1, Deutsches Patent- und Markenamt, 1–18.
2. Matz, M. V., A. F. Fradkov, Y. A. Labas, A. P. Savitsky, A. G. Zaraisky, M. L. Markelov, and S. A. Lukyanov. 1999. Fluorescent proteins from nonbioluminescent Anthozoa species. *Nat. Biotechnol.* 17:969–973.
3. Wiedenmann, J., C. Elke, K. D. Spindler, and W. Funke. 2000. Cracks in the beta-can: fluorescent proteins from Anemonia sulcata (Anthozoa, Actinaria). *Proc. Natl. Acad. Sci. USA.* 97:14091–14096.
4. Shagin, D. A., E. V. Barsova, Y. G. Yanushevich, A. F. Fradkov, K. A. Lukyanov, Y. A. Labas, T. N. Semenova, J. A. Ugalde, A. Meyers, J. M. Nunez, E. A. Widder, S. A. Lukyanov, and M. V. Matz. 2004. GFP-like proteins as ubiquitous metazoan superfamily: evolution of functional features and structural complexity. *Mol. Biol. Evol.* 21:841–850.
5. Dove, S. G., O. Hoegh-Guldberg, and S. Ranganathan. 2001. Major colour patterns of reef-building corals are due to a family of GFP-like proteins. *Coral Reefs.* 19:197–204.
6. Ormö, M., A. B. Cubitt, K. Kallio, L. A. Gross, R. Y. Tsien, and S. J. Remington. 1996. Crystal structure of the Aequorea victoria green fluorescent protein. *Science.* 273:1392–1395.
7. Yang, F., L. G. Moss, and G. N. Phillips Jr. 1996. The molecular structure of green fluorescent protein. *Nat. Biotechnol.* 14: 1246–1251.
8. Prasher, D. C., V. K. Eckenrode, W. W. Ward, F. G. Prendergast, and M. J. Cormier. 1992. Primary structure of the Aequorea victoria green-fluorescent protein. *Gene.* 111:229–233.
9. Tsien, R. Y. 1998. The green fluorescent protein. *Annu. Rev. Biochem.* 67:509–544.
10. Reid, B. G., and G. C. Flynn. 1997. Chromophore formation in green fluorescent protein. *Biochemistry.* 36:6786–6791.
11. Heim, R., D. C. Prasher, and R. Y. Tsien. 1994. Wavelength mutations and posttranslational autoxidation of green fluorescent protein. *Proc. Natl. Acad. Sci. USA.* 91:12501–12504.
12. Waldo, G. S., B. M. Standish, J. Berendzen, and T. C. Terwilliger. 1999. Rapid protein-folding assay using green fluorescent protein. *Nat. Biotechnol.* 17:691–695.
13. Romoser, V. A., P. M. Hinkle, and A. Persechini. 1997. Detection in living cells of Ca2+-dependent changes in the fluorescence emission of an indicator composed of two green fluorescent protein variants linked by a calmodulin-binding sequence. A new class of fluorescent indicators. *J. Biol. Chem.* 272:13270–13274.
14. Kneen, M., J. Farinas, Y. Li, and A. S. Verkman. 1998. Green fluorescent protein as a noninvasive intracellular pH indicator. *Biophys. J.* 74:1591–1599.
15. Miyawaki, A., J. Llopis, R. Heim, J. M. McCaffery, J. A. Adams, M. Ikura, and R. Y. Tsien. 1997. Fluorescent indicators for Ca2+ based on green fluorescent proteins and calmodulin. *Nature.* 388:882–887.
16. Barondeau, D. P., C. J. Kassmann, J. A. Tainer, and E. D. Getzoff. 2002. Structural chemistry of a green fluorescent protein Zn biosensor. *J. Am. Chem. Soc.* 124:3522–3524.
17. Remington, S. J. 2000. Structural basis for understanding spectral variations in green fluorescent protein. *Methods Enzymol.* 305:196–211.
18. Palm, G. J., A. Zdanov, G. A. Gaitanaris, R. Stauber, G. N. Pavlakis, and A. Wlodawer. 1997. The structural basis for spectral variations in green fluorescent protein. *Nat. Struct. Biol.* 4:361–365.
19. Heim, R., A. B. Cubitt, and R. Y. Tsien. 1995. Improved green fluorescence. *Nature.* 373:663–664.
20. Yarbrough, D., R. M. Wachter, K. Kallio, M. V. Matz, and S. J. Remington. 2001. Refined crystal structure of DsRed, a red fluorescent protein from coral, at 2.0-Å resolution. *Proc. Natl. Acad. Sci. USA.* 98:462–467.
21. Campbell, R. E., O. Tour, A. E. Palmer, P. A. Steinbach, G. S. Baird, D. A. Zacharias, and R. Y. Tsien. 2002. A monomeric red fluorescent protein. *Proc. Natl. Acad. Sci. USA.* 99:7877–7882.
22. Gross, L. A., G. S. Baird, R. C. Hoffman, K. K. Baldridge, and R. Y. Tsien. 2000. The structure of the chromophore within DsRed, a red fluorescent protein from coral. *Proc. Natl. Acad. Sci. USA.* 97:11990–11995.
23. Petersen, J., P. G. Wilmann, T. Beddoe, A. J. Oakley, R. J. Devenish, M. Prescott, and J. Rossjohn. 2003. The 2.0-Å crystal structure of eqFP611, a far red fluorescent protein from the sea anemone Entacmaea quadricolor. *J. Biol. Chem.* 278:44626–44631.
24. Nienhaus, K., B. Vallone, F. Renzi, J. Wiedenmann, and G. U. Nienhaus. 2003. Crystallization and preliminary x-ray diffraction analysis of the red fluorescent protein eqFP611. *Acta Crystallogr. D.* 59:1253–1255.
25. Ando, R., H. Hama, M. Yamamoto-Hino, H. Mizuno, and A. Miyawaki. 2002. An optical marker based on the UV-induced green-to-red photoconversion of a fluorescent protein. *Proc. Natl. Acad. Sci. USA.* 99:12651–12656.
26. Mizuno, H., T. K. Mal, K. I. Tong, R. Ando, T. Furuta, M. Ikura, and A. Miyawaki. 2003. Photo-induced peptide cleavage in the green-to-red conversion of a fluorescent protein. *Mol. Cell.* 12:1051–1058.

27. Wiedenmann, J., S. Ivanchenko, F. Oswald, F. Schmitt, C. Röcker, A. Salih, K. D. Spindler, and G. U. Nienhaus. 2004. EosFP, a fluorescent marker protein with UV-inducible green-to-red fluorescence conversion. *Proc. Natl. Acad. Sci. USA.* 101:15905–15910.

28. Nienhaus, K., G. U. Nienhaus, J. Wiedenmann, and H. Nar. 2005. Structural basis for photo-induced protein cleavage and green-to-red conversion of fluorescent protein EosFP. *Proc. Natl. Acad. Sci. USA.* 102:9156–9159.

29. Wiedenmann, J., and G. U. Nienhaus. 2006. Live-cell imaging with EosFP and other photoactivatable marker proteins of the GFP family. *Expert Rev. Proteomics.* 3:361–374.

30. Wiedenmann, J., B. Vallone, F. Renzi, K. Nienhaus, S. Ivanchenko, C. Röcker, and G. U. Nienhaus. 2005. Red fluorescent protein eqFP611 and its genetically engineered dimeric variants. *J. Biomed. Opt.* 10:14003.

31. Miyawaki, A., T. Nagai, and H. Mizuno. 2005. Engineering fluorescent proteins. *Adv. Biochem. Eng. Biotechnol.* 95:1–15.

32. Wang, Z., J. V. Shah, Z. Chen, C. H. Sun, and M. W. Berns. 2004. Fluorescence correlation spectroscopy investigation of a GFP mutant-enhanced cyan fluorescent protein and its tubulin fusion in living cells with two-photon excitation. *J. Biomed. Opt.* 9:395–403.

33. Ivanchenko, S., C. Röcker, F. Oswald, J. Wiedenmann, and G. U. Nienhaus. 2005. Targeted green-to-red photoconversion of EosFP, a fluorescent marker protein. *J. Biol. Phys.* 31:249–259.

34. Wiedenmann, J., S. Ivanchenko, F. Oswald, and G. U. Nienhaus. 2004. Identification of GFP-like proteins in nonbioluminescent, Azooxanthellate Anthozoa opens new perspectives for bioprospecting. *Mar. Biotechnol. (NY).* 6:270–277.

35. Otwinowski, Z., and W. Minor. 1997. Data collection and processing. *Methods Enzymol.* 276:307–326.

36. Bailey, S. 1994. The CCP4 suite: programs for protein crystallography. *Acta Crystallogr. D.* 50:760–763.

37. QUANTA software. School of Crystallography, B. C., University of London, London, United Kingdom.

38. Emsley, P., and K. Kowtan. 2004. COOT version 0.026 model building and molecular graphics system. *Acta Crystallogr. D.* 70:2126–2132.

39. PyMOL version 0.97 Molecular Graphics System. DeLano Scientific, South San Francisco, CA.

40. Sniegowski, J. A., J. W. Lappe, H. N. Patel, H. A. Huffman, and R. M. Wachter. 2005. Base catalysis of chromophore formation in Arg96 and Glu222 variants of green fluorescent protein. *J. Biol. Chem.* 280: 26248–26255.

41. Wood, T. I., D. P. Barondeau, C. Hitomi, C. J. Kassmann, J. A. Tainer, and E. D. Getzoff. 2005. Defining the role of arginine 96 in green fluorescent protein fluorophore biosynthesis. *Biochemistry.* 44:16211–16220.

42. Wachter, R. M., M. A. Elsliger, K. Kallio, G. T. Hanson, and S. J. Remington. 1998. Structural basis of spectral shifts in the yellow-emission variants of green fluorescent protein. *Structure.* 6: 1267–1277.

43. Wiedenmann, J., A. Schenk, C. Röcker, A. Girod, K. D. Spindler, and G. U. Nienhaus. 2002. A far-red fluorescent protein with fast maturation and reduced oligomerization tendency from Entacmaea quadricolor (Anthozoa, Actinaria). *Proc. Natl. Acad. Sci. USA.* 99: 11646–11651.

44. Nienhaus, G. U., K. Nienhaus, A. Hölzle, S. Ivanchenko, F. Renzi, F. Oswald, M. Wolff, F. Schmitt, C. Röcker, B. Vallone, W. Weidemann, R. Heilker, H. Nar, and J. Wiedenmann. 2005. Photoconvertible fluorescent protein EosFP-biophysical properties and cell biology applications. *Photochem. Photobiol.* 82:351–358.

45. Jung, G., J. Wiehler, and A. Zumbusch. 2005. The photophysics of green fluorescent protein: influence of the key amino acids at positions 65, 203, and 222. *Biophys. J.* 88:1932–1947.

46. Elsliger, M. A., R. M. Wachter, G. T. Hanson, K. Kallio, and S. J. Remington. 1999. Structural and spectral response of green fluorescent protein variants to changes in pH. *Biochemistry.* 38:5296–5301.

47. Chattoraj, M., B. A. King, G. U. Bublitz, and S. G. Boxer. 1996. Ultra-fast excited state dynamics in green fluorescent protein: multiple states and proton transfer. *Proc. Natl. Acad. Sci. USA.* 93: 8362–8367.

48. Creemers, T. M. H., A. J. Lock, V. Subramaniam, T. M. Jovin, and S. Völker. 1999. Three photoconvertible forms of green fluorescent protein identified by spectral hole-burning. *Nat. Struct. Biol.* 6: 557–560.

49. Ward, W. W., and S. H. Bokman. 1982. Reversible denaturation of Aequorea green-fluorescent protein: physical separation and characterization of the renatured protein. *Biochemistry.* 21:4535–4540.

50. Ward, W. W., H. J. Prentice, A. F. Roth, C. W. Cody, and S. C. Reeves. 1982. Spectral perturbations of the *Aequorea* green-fluorescent protein. *Photochem. Photobiol.* 35:803–808.

51. Weber, W., V. Helms, J. A. McCammon, and P. W. Langhoff. 1999. Shedding light on the dark and weakly fluorescent states of green fluorescent proteins. *Proc. Natl. Acad. Sci. USA.* 96:6177–6182.

52. Voityuk, A. A., M. E. Michel-Beyerle, and N. Rösch. 1998. Quantum chemical modeling of structure and absorption spectra of the chromophore in green fluorescent proteins. *Chem. Phys.* 231:13–25.

53. Cubitt, A. B., R. Heim, S. R. Adams, A. E. Boyd, L. A. Gross, and R. Y. Tsien. 1995. Understanding, improving and using green fluorescent proteins. *Trends Biochem. Sci.* 20:448–455.

54. Zimmer, M. 2002. Green fluorescent protein (GFP): applications, structure, and related photophysical behavior. *Chem. Rev.* 102: 759–781.

55. Wiehler, J., G. Jung, C. Seebacher, A. Zumbusch, and B. Steipe. 2003. Mutagenic stabilization of the photocycle intermediate of green fluorescent protein (GFP). *ChemBioChem.* 4:1164–1171.

56. Brejc, K., T. K. Sixma, P. A. Kitts, S. R. Kain, R. Y. Tsien, M. Ormo, and S. J. Remington. 1997. Structural basis for dual excitation and photoisomerization of the Aequorea victoria green fluorescent protein. *Proc. Natl. Acad. Sci. USA.* 94:2306–2311.

57. Scharnagl, C., R. Raupp-Kossmann, and S. F. Fischer. 1999. Molecular basis for pH sensitivity and proton transfer in green fluorescent protein: protonation and conformational substates from electrostatic calculations. *Biophys. J.* 77:1839–1857.

58. Schellenberg, P., E. Johnson, A. P. Esposito, P. J. Reid, and W. W. Parson. 2001. Resonance Raman scattering by the green fluorescent protein and an analogue of its chromophore. *J. Phys. Chem. B.* 105: 5316–5322.

59. He, X., A. F. Bell, and P. J. Tonge. 2002. Isotopic labeling and normal-mode analysis of a model green fluorescent protein chromophore. *J. Phys. Chem. B.* 106:6056–6066.

60. Gurskaya, N. G., A. P. Savitsky, Y. G. Yanushevich, S. A. Lukyanov, and K. A. Lukyanov. 2001. Color transitions in coral's fluorescent proteins by site-directed mutagenesis. *BMC Biochem.* 2:6.

61. Sinicropi, A., T. Andruniow, N. Ferre, R. Basosi, and M. Olivucci. 2005. Properties of the emitting state of the green fluorescent protein resolved at the CASPT2//CASSCF/CHARMM level. *J. Am. Chem. Soc.* 127:11534–11535.

62. Tozzini, V., and R. Nifosi. 2001. Ab initio molecular dynamics of the green fluorescent protein (GFP) chromophore: an insight into the photoinduced dynamics of green fluorescent proteins. *J. Phys. Chem. B.* 105:5797–5803.

63. Marques, M. A., X. Lopez, D. Varsano, A. Castro, and A. Rubio. 2003. Time-dependent density-functional approach for biological chromophores: the case of the green fluorescent protein. *Phys. Rev. Lett.* 90:258101.

64. Cinelli, R. A., V. Tozzini, V. Pellegrini, F. Beltram, G. Cerullo, M. Zavelani-Rossi, S. De Silvestri, M. Tyagi, and M. Giacca. 2001. Coherent dynamics of photoexcited green fluorescent proteins. *Phys. Rev. Lett.* 86:3439–3442.

65. Müller, J. D., B. H. McMahon, E. Y. Chien, S. G. Sligar, and G. U. Nienhaus. 1999. Connection between the taxonomic substates and protonation of histidines 64 and 97 in carbonmonoxy myoglobin. *Biophys. J.* 77:1036–1051.

66. Nienhaus, K., J. M. Kriegl, and G. U. Nienhaus. 2004. Structural dynamics in the active site of murine neuroglobin and its effects on ligand binding. *J. Biol. Chem.* 279:22944–22952.

67. Creemers, T. M. H., A. J. Lock, V. Subramaniam, T. M. Jovin, and S. Völker. 2000. Photophysics and optical switching in green fluorescent protein mutants. *Proc. Natl. Acad. Sci. USA.* 97:2974–2978.

68. Cotlet, M., J. Hofkens, M. Maus, T. Gensch, M. Van der Auweraer, J. Michiels, G. Dirix, M. Van Guyse, J. Vanderleyden, A. Visser, and F. C. De Schryver. 2001. Excited-state dynamics in the enhanced green fluorescent protein mutant probed by picosecond time-resolved single photon counting spectroscopy. *J. Phys. Chem. B.* 105:4999–5006.

69. Striker, G., V. Subramaniam, C. A. M. Seidel, and A. Volkmer. 1999. Photochromicity and fluorescence lifetimes of green fluorescent protein. *J. Phys. Chem. B.* 103:8612–8617.

70. Seebacher, C., F. W. Deeg, C. Brauchle, J. Wiehler, and B. Steipe. 1999. Stable low-temperature photoproducts and hole burning of green fluorescent protein (GFP). *J. Phys. Chem. B.* 103:7728–7732.